

PREDICTION OF FLOOD INUNDATION FROM
BREACHED DAMS DUE TO EARTHQUAKES

D. L. Fread

Office of Hydrology, National Weather Service

ABSTRACT

Dam failures caused by earthquakes present a potential for catastrophic downstream flooding. A mathematical model for predicting the time of occurrence and extent of downstream inundation is presented. The math model (DAMBRK) represents the state-of-the-art; it provides for a time dependent dam breach with variable geometry and considers the simultaneous effects on the reservoir outflow of reservoir storage, reservoir inflows, spillway outflows, and tailwater elevation. The outflow is routed through the downstream valley via an implicit finite difference solution of the complete one-dimensional equations of unsteady flow. Effects of downstream bridges, dams, floodplains, and channel sinuosity can be considered. Applications of the model to the 1976 Teton Dam and 1972 Buffalo Creek floods are presented. Computed Peak elevations agreed with observed values within an average of 1.5 to 1.8 feet. Both applications indicated an important lack of sensitivity of downstream peak discharge to reasonable errors in the breach size and failure time. Such errors produced significant differences in the peak discharge in the vicinity of the dams; however, the differences were rapidly reduced as the wave advanced downstream. Computer simulation time was quite modest; approximately 20 seconds was required on an IBM 360/195 for each flood simulation.

1. INTRODUCTION

Dam failures as reported by Middlebrooks (1952) and Johnson and Illes (1976) may be caused by damage sustained by the structure during an earthquake. The water released by the failure of the dam has the potential for large-scale destruction if the dam is located less than a few miles upstream of populated areas. The devastation to the downstream valley is due to the substantial magnitude of the flood wave emanating from the breached dam. Such a flood wave usually exceeds the previous flood by as much as an order of magnitude. The dam-break flood wave is of substantial depth (as much as 25 to 40 percent of the reservoir depth). It has high flow velocities which destroy almost everything in its path for the first few miles downstream of the dam. Trees are uprooted, large boulders and huge quantities of sediment are transported, buildings, bridges, and other

improvements of man are destroyed. Inundation never before experienced can persist as far downstream as 60 miles as in the Teton Dam flood of 1976. Such flooding could even extend farther downstream for dam failures where the reservoir is larger than the Teton Reservoir which was 260 feet deep with 250,000 acre-ft of stored water.

Earthquakes may also generate landslides. If the landslide occurs on the banks of a reservoir, the landslide mass rushes into the reservoir displacing its volume of water which then propagates throughout the length of the reservoir as a large, steep-fronted water wave. When the wave impinges on the dam it can cause failure of the structure. However, it is possible as in the Italian Vialto Dam flood of 1963 for the structure to sustain little damage yet the volume of the overtopping wave is large enough to produce catastrophic flooding below the dam.

1.1 Potential damage due to earthquake-generated flooding

In the brief history of the United States, major earthquakes have occurred in the West, Central, and East. Although the frequency of occurrence is greater in the West, the severity of any individual earthquake can be just as great in the Central (New Madrid, Missouri earthquakes of 1811-12) or in the East (Charleston, South Carolina earthquake of 1886). Unless specifically controlled, it is customary to neglect the need for earthquake resistant construction in low risk areas. Expansion of economic activities into potentially vulnerable areas with accompanying increases in population density can result in earthquake catastrophes that were not possible a few years ago. The Nation could face substantial losses of life and properties if a catastrophic earthquake would generate large-scale flooding from dam failures. Studies have estimated the potential loss of life in the range of 2,000 to 100,000 and property loss in the billions of dollars with even greater losses in productivity and earnings. Damage and lives lost in future earthquake-generated flooding can be expected to be more and more devastating because of continuous construction and population growth.

Numerous dams exist in all sections of the country. The potential for catastrophic flooding due to dam failures has recently been brought to the Nation's attention by several non-earthquake-generated dam failures such as the 1972 Buffalo Creek coal-waste dam flood, the 1976 Teton Dam flood, the 1977 Toccoa Georgia flood, and the 1977 Laurel Run Dam flood in Pennsylvania. A report by the U.S. Army (1975) gives an inventory of the Nation's approximately 50,000 dams with heights greater than 25 feet or storage volumes in excess of 50 acre-ft. The report also classifies some 20,000 of these as being "so located that failure of the dam could result in loss of human life and appreciable property damage..."

1.2 Earthquake effects on earthen dams

Embankment failures can be initiated by earthquakes of magnitudes as low as 5 or peak accelerations around 0.2 g. and above. There is a substantial difference between the seismic resistance of embankments composed of clayey or cohesive soils and those consisting of saturated sands or other non-cohesive soils. Generally, embankments composed of cohesive

soils can withstand extremely strong earth shaking (normally 0.35 g. to 0.8 g. or magnitudes of 8 or more). Cohesionless materials existing in fills or slopes in a saturated condition are particularly vulnerable to failure when subjected to shaking. The earthquake shaking of a wet sandy type material can make it behave like a fluid. This liquefaction of the foundation of an embankment may result in subsidence and/or collapse. When embankments composed of cohesionless soil remains stable under shaking, it can usually be attributed to the lack of saturation.

Usually, the principal damage to a dam embankment is caused by the horizontal component of the earthquake in the upstream-downstream direction. The amplitude and acceleration of the horizontal component of the movement at the crest of the dam is much larger than the movement at the base which results in a whipping action of the thinner top and creating longitudinal cracks. Therefore, the normal damage is usually longitudinal cracks at the top of the embankment and crest settlement. The impounded water may then escape through the cracks eroding them into larger gaps causing the dam to be breached. Dams with cores are usually more badly cracked than dams without cores. Earthquakes are also accompanied by localized land subsidence that can cause serious cracking of the dam.

Loose uncompacted fill materials are more seriously affected by earthquake shocks. They are literally shaken to pieces, settle as much as 50 percent, spread at the base, and develop large cracks in all directions. In this case the erosion process by which the breach is formed is more rapid and the size of the breach is likely to be greater than for well-compacted embankments.

1.3 Prediction of flood inundation from breached dams

Techniques or mathematical models for computing the extent of inundation from precipitation runoff-generated flood waves progressing through a valley are well-established having been used by hydrologists and hydraulic engineers for many years. Although the dam-break wave has many similarities to runoff-generated flood waves, it also has some very important differences which make it difficult to analyze with the common techniques which have worked satisfactorily for the precipitation-runoff floods. To aid flood hydrologists and engineers who are called upon to predict the downstream flooding (flood inundation information and warning times) resulting from dam failures, a numerical math model (DAMBRK) has been recently developed by the National Weather Service. This model has gained wide acceptance within the engineering community and is currently being used by many federal and state agencies as well as many private consultants. The model is representative of the best state-of-the-art techniques for predicting dam-failure flood inundation. Its theoretical basis and predictive capabilities are presented herein as a recommended technique. The DAMBRK model can be used for real-time flood forecasting, engineering planning and design, and evacuation planning associated with dam-break flood inundation. The model is applied to the catastrophic floods which resulted from the Teton Dam failure and the collapse of the Buffalo Creek coal-waste dam to test its predictive capabilities and parameter sensitivities.

2. MODEL DEVELOPMENT

The DAMBRK model represents the current state-of-the-art in understanding of dam failures and the utilization of hydrodynamic theory to predict the dam-break wave formation and downstream progression. The model has wide applicability; it can function with various levels of input data ranging from rough estimates to complete data specification; the required data is readily accessible; and it is economically feasible to use, i.e., it requires a minimal computational effort on large computing facilities.

The model consists of three functional parts, namely: (1) description of the dam failure mode, i.e., the temporal and geometrical description of the breach; (2) computation of the time history (hydrograph) of the outflow through the breach as affected by the breach description, reservoir inflow, reservoir storage characteristics, spillway outflows, and downstream tailwater elevations; and (3) routing of the outflow hydrograph through the downstream valley in order to determine the changes in the hydrograph due to valley storage, frictional resistance, downstream bridges or dams, and to determine the resulting water surface elevations (stages) and flood-wave travel times.

DAMBRK is an expanded version of a practical operational model first presented in 1977 by the author (Fread, 1977). That model was based on previous work by the author on modeling breached dams (Fread and Harbaugh, 1973) and routing of flood waves (Fread, 1974, 1976). There have been a number of other operational dam-break models that have appeared recently in the literature, e.g., Price, et al. (1977), Gundlach and Thomas (1977), Thomas (1977), Keefer and Simons (1977), Chen and Druffel (1977), Balloffet, et al. (1974), Balloffet (1977), Brown and Rogers (1977), Rajar (1978), Brevard and Theurer (1979). DAMBRK differs from each of these models in the treatment of the breach formation, the outflow hydrograph generation, and the downstream flood routing.

2.1 Breach Description

The breach is the opening formed in the dam as it fails. The actual failure mechanics are not well understood for either earthen or concrete dams. In previous attempts to predict downstream flooding due to dam failures, it was usually assumed that the dam failed completely and instantaneously. Investigators of dam-break flood waves such as Ritter (1892), Schocklitsch (1891), Ré (1946), Dressler (1954), Stoker (1957), Su and Barnes (1969), and Sakkas and Strelkoff (1973) assumed the breach encompasses the entire dam and that it occurs instantaneously. Others, such as Schocklitz (1891) and Army Corps of Engineers (1960, 1961), have recognized the need to assume partial rather than complete breaches; however, they assumed

the breach occurred instantaneously. The assumptions of instantaneous and complete breaches were used for reasons of convenience when applying certain mathematical techniques for analyzing dam-break flood waves. These assumptions are somewhat appropriate for concrete arch-type dams, but they are not appropriate for earthen dams and concrete gravity-type dams.

Earthen dams which exceedingly outnumber all other types of dams do not tend to completely fail, nor do they fail instantaneously. The fully formed breach in earthen dams tends to have an average width (\bar{b}) in the range ($h_d < \bar{b} < 3h_d$) where h_d is the height of the dam. The middle portion of this range for \bar{b} is supported by the summary report of Johnson and Illes (1976). Breach widths for earthen dams are therefore usually much less than the total length of the dam as measured across the valley. Also, the breach requires a finite interval of time for its formation through erosion of the dam materials by the escaping water. Total time of failure may be in the range of a few minutes to a few hours, depending on the height of the dam, the type of materials used in construction, the extent of compaction of the materials, and the extent (magnitude and duration) of the overtopping flow of the escaping water. Piping failures occur when initial breach formation takes place at some point below the top of the dam due to erosion of an internal channel through the dam by escaping water. As the erosion proceeds, a larger and larger opening is formed; this is eventually hastened by caving-in of the top portion of the dam. Earthquake-damaged dams, where erosion of the earthquake-generated cracks cause the dam to fail, would tend to behave in a similar manner to overtopping or piping failures.

Concrete gravity dams also tend to have a partial breach as one or more monolith sections formed during the construction of the dam are forced apart by the escaping water. The time for breach formation is in the range of a few minutes.

Poorly constructed earthen dams, coal-waste slag piles which impound water, and dam failures due to earthquake-liquefaction of the embankment materials tend to fail within a few minutes, and have average breach widths in the upper range or even greater than those for the earthen dams mentioned above.

Cristofano (1965) attempted to model the partial, time-dependent breach formation in earthen dams; however, this procedure requires critical assumptions and specification of unknown critical parameter values. Also, Harris and Wagner (1967) used a sediment transport relation to determine the time for breach formation, but this procedure requires specification of breach size and shape in addition to two critical parameters for the sediment transport relation.

For reasons of simplicity, generality, wide applicability, and the uncertainty in the actual failure mechanism, the NWS DAMBRK model allows the model user to input the failure time interval (τ) and the terminal size and shape of the breach (Fread and Harbaugh, 1973). The shape

(see Fig. 1) is specified by a parameter (z) identifying the side slope of the breach, i.e., 1 vertical: z horizontal slope. The range of z values is : $0 \leq z \leq 2$. Rectangular, triangular, or trapezoidal shapes

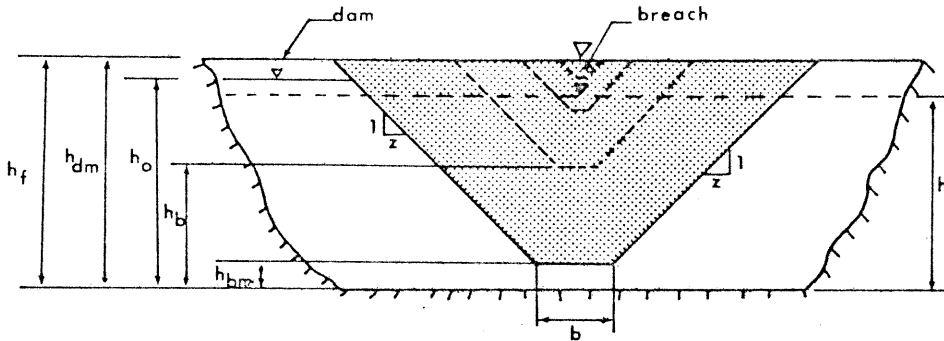


Fig.1- FRONT VIEW OF DAM SHOWING FORMATION OF BREACH

may be specified in this way. For example, $z=0$ and $b>0$ produces a triangular shape; and $z>0$, $b>0$ produces a trapezoidal shape. The final breach size is controlled by the z parameter and another parameter (b) which is the terminal width of the bottom of the breach. As shown in Fig. 1, the model assumes the breach bottom width starts at a point and enlarges at a linear rate over the failure time interval (τ) until the terminal width is attained and the breach bottom has eroded to the elevation h_{bm} which is usually, but not necessarily, the bottom of the reservoir or outlet channel bottom. If τ is less than 10 minutes, the width of the breach bottom starts at a value of b rather than at a point. This represents more of a collapse failure than an erosion failure.

During the simulation of a dam failure, the actual breach formation commences when the reservoir water surface elevation (h) exceeds a specified value, h_f . This feature permits the simulation of an overtopping of a dam in which the breach does not form until a sufficient amount of water is flowing over the crest of the dam. A piping failure may be simulated when h_f is specified less than the height of the dam, h_d . For earthquake generated failures the failure may most likely commence at the normal operating pool level (h) and the height of the dam (h_d) is considered to be same as h ; therefore, $h_f = h_d = h$.

Selection of breach parameters before a breach forms, or in the absence of observations, introduces a varying degree of uncertainty in the model results; however, errors in the breach description and thence in the resulting time rate of volume outflow are rapidly damped-out as the flood wave advances downstream. For conservative predictions which err on the side of larger flood waves, values for b and z should produce an average breach width (\bar{b}) in the uppermost range for a certain

type of dam. Failure time (τ) should be selected in the lower range to produce a maximum outflow. Flood wave travel rates are often in the range of 2-10 miles per hour. Accordingly, response times for some downstream forecast points may therefore be sufficient for updated forecasts to be issued.

2.2 Reservoir Outflow Hydrograph

The total reservoir outflow consists of broad-crested weir flow through the breach and flow through any spillway outlets, i.e.,

$$Q = Q_b + Q_s \quad (1)$$

The breach outflow (Q_b) is computed as:

$$Q_b = c_1 (h-h_b)^{1.5} + c_2 (h-h_b)^{2.5} \quad (2)$$

where:

$$c_1 = 3.1 b_i c_v k_s \quad (3)$$

$$c_2 = 2.45 z c_v k_s \quad (4)$$

$$h_b = h_d - (h_d - h_{bm}) \frac{t_b}{\tau} \quad \text{if} \quad t_b \leq \tau \quad (5)$$

$$h_b = h_{bm} \quad \text{if} \quad t_b \geq \tau \quad (6)$$

$$b_i = b t_b / \tau \quad \text{if} \quad t_b \leq \tau \quad (7)$$

$$c_v = 1.0 + 0.023 Q^2 / [B_d^2 h^2 (h-h_b)] \quad (8)$$

$$k_s = 1.0 \quad \text{if} \quad \frac{h_t - h_b}{h - h_b} \leq 0.67 \quad (9)$$

otherwise:

$$k_s = 1.0 - 27.8 \left[\frac{h_t - h_b}{h - h_b} - 0.67 \right]^3 \quad (10)$$

in which h_b is the elevation of the breach bottom, h is the reservoir water surface elevation, b_i is the instantaneous breach bottom width, t_b is time interval since breach started forming, c_v is correction for velocity of approach (Brater, 1959), Q is the total outflow from the reservoir, B_d is width of the reservoir at the dam, k_s is the submergence correction for tailwater effects on weir outflow (Venard, 1954), and h_t is the tailwater elevation (water surface elevation immediately downstream of dam).

The tailwater elevation (h_t) is computed from Manning's equation, i.e.,

$$Q = \frac{1.49}{n} S^{1/2} \frac{A^{5/3}}{B^{2/3}} \quad (11)$$

in which n is the Manning roughness coefficient, A is the cross-sectional area of flow, B is the top width of the wetted cross-sectional area, and S is the energy slope. Each term in Eq. (11) applies to a representative channel reach immediately downstream of the dam. The S parameter can be specified by the user; it does not change with time; if it is not specified, the model uses the channel bottom slope of the first third of the downstream valley reach. Since A and B are functions of h_t and Q is the total discharge given by Eq. (1), Eq. (11) can be solved for h_t using Newton-Raphson iteration. Eq. (11) provides a sufficiently accurate value for h_t if there are no backwater effects immediately below the dam due to downstream constrictions, dams, bridges, or significant tributary inflows. When these affect the tailwater, Eq. (11) is not used and another procedure, referred to herein as the "simultaneous method," which is described in a following section on multiple dams and bridges is used.

If the breach is formed by piping, Eq. (2)-(9) are replaced by the following orifice flow equation:

$$Q_b = 4.8 A_p (h - \bar{h})^{1/2} \quad (12)$$

where:

$$A_p = [2b_i + 4z(h_f - h_b)] (h_f - h_b) \quad (13)$$

$$\bar{h} = h_f \quad \text{if} \quad h_t \leq 2h_f - h_b \quad (14)$$

$$\bar{h} = h_t \quad \text{if} \quad h_t > 2h_f - h_b \quad (15)$$

and h_d is replaced by h_f in Eq. (5) to compute h_b .

However, if $\bar{h} = h_f$ and

$$h - h_b < 3(h_f - h_b) \quad (16)$$

the flow ceases to be orifice flow and the broad-crested weir flow, Eq. (2), is used.

The spillway outflow (Q_s) is computed as:

$$Q_s = c_s L_s (h - h_s)^{1.5} + c_g A_g (h - h_g)^{0.5} + c_d L_d (h - h_d)^{1.5} + Q_t \quad (17)$$

in which c_s is the uncontrolled spillway discharge coefficient, h_s is the uncontrolled spillway crest elevation, c_g is the gated spillway discharge coefficient, h_g is the center-line elevation of the gated spillway, c_d is the discharge coefficient for flow over the crest of the dam, L_s is the spillway length, A_g is the gate flow area, L_d is the length of the dam crest less L_s , and Q_t is a constant outflow term which is head independent. The uncontrolled spillway flow or the gated spillway flow can also be represented as a table of head-discharge values.

The total outflow is a function of the water surface elevation (h). Depletion of the reservoir storage volume by the outflow causes a decrease in h which then causes a decrease in Q . However, any inflow to the reservoir tends to increase h and Q . In order to determine the total outflow (Q) as function of time, the simultaneous effects of reservoir storage characteristics and reservoir inflow require the use of a reservoir routing technique. DAMBRK utilizes a hydrologic storage routing technique based on the law of conservation of mass, i.e.,

$$I - Q = dS/dt \quad (18)$$

in which I is the reservoir inflow, Q is the total reservoir outflow, and dS/dt is the time rate of change of reservoir storage volume. Eq. (18) may be expressed in finite difference form as:

$$(I+I')/2 - (Q+Q')/2 = \Delta S/\Delta t \quad (19)$$

in which the prime (') superscript denotes values at the time $t-\Delta t$ and the Δ approximates the differential. The term ΔS may be expressed as:

$$\Delta S = (A_s + A'_s) (h - h')/2 \quad (20)$$

in which A_s is the reservoir surface area coincident with the elevation (h).

Combining Eqs. (1), (2), (17), (19) and (20) result in the following expression:

$$(A_s + A'_s) (h - h') / \Delta t + c_1 (h - h_b)^{1.5} + c_2 (h - h_b)^{2.5} + c_s (h - h_b)^{1.5} + c_g (h - h_g)^{0.5} + c_d (h - h_d)^{1.5} + Q_t + Q' - I - I' = 0 \quad (21)$$

Since A_s is a function of h and all other terms except h are known, Eq. (21) can be solved for the unknown h using Newton-Raphson iteration. Having obtained h , usually within two or three iterations, Eqs. (2) and (17) can be used to obtain the total outflow (Q) at time (t). In this way the outflow hydrograph $Q(t)$ can be developed for each time (t) as t goes from zero to some terminating value (t_e) sufficiently large for the reservoir to be drained. In Eq. (21) the time step (Δt) is chosen sufficiently small to incur minimal numerical integration error. This value is preset in the model to $\tau/50$.

The hydrologic storage routing technique, Eq. (18), implies that the water surface elevation within the reservoir is level. This assumption is quite adequate for gradually occurring breaches with no substantial reservoir inflow hydrographs. However, when 1) the breach is specified to form almost instantaneously so as to produce a negative wave within the reservoir, and/or 2) the reservoir inflow hydrograph is significant enough to produce a positive wave progressing through the reservoir, a routing technique which simulates the negative and/or positive wave(s) occurring within the reservoir could be used for greater accuracy in computing the reservoir outflow through the breach and/or spillways. Such a technique is referred to as dynamic routing. Since this technique is used for routing the dam-break flood wave through the downstream valley, the application of it in lieu of reservoir storage routing will be presented after the downstream routing technique is presented.

2.3 Downstream Routing

After computing the hydrograph of the reservoir outflow, the extent of and time of occurrence of flooding in the downstream valley is determined by routing the outflow hydrograph through the valley. The hydrograph is modified (attenuated, lagged, and distorted) as it is routed through the valley due to the effects of valley storage, frictional resistance to flow, flood wave acceleration components, and downstream obstructions and/or flow control structures. Modifications to the dam-break flood wave are manifested as attenuation of the flood peak elevation, spreading-out or dispersion of the flood wave volume, and changes in the celerity (translation speed) or travel time of the flood wave. If the downstream valley contains significant storage volume such as a wide flood plain, the flood wave can

be extensively attenuated and its time of travel greatly increased. Even when the downstream valley approaches that of a uniform rectangular-shaped section, there is appreciable attenuation of the flood peak and reduction in the wave celerity as the wave progresses through the valley.

A distinguishing feature of dam-break waves is the great magnitude of the peak discharge when compared to runoff-generated flood waves having occurred in the past in the same valley. The dam-break flood is usually many times greater than the runoff flood of record. The above-record discharges make it necessary to extrapolate certain coefficients used in various flood routing techniques and make it impossible to fully calibrate the routing technique.

Another distinguishing characteristic of dam-break floods is the very short duration time, and particularly the extremely short time from beginning of rise until the occurrence of the peak. The time to peak is in almost all instances synonymous with the breach formation time (τ) and therefore is in the range of a few minutes to a few hours. This feature, coupled with the great magnitude of the peak discharge, causes the dam-break flood wave to have acceleration components of a far greater significance than those associated with a runoff-generated flood wave.

There are two basic types of flood routing methods, the hydrologic and the hydraulic methods. The hydrologic methods are more of an approximate analysis of the progression of a flood wave through a river reach than are the hydraulic methods. The hydrologic methods are used for reasons of convenience and economy. They are most appropriate as far as accuracy is concerned when the flood wave is not rapidly varying, i.e., the flood wave acceleration effects are negligible compared to the effects of gravity and channel friction. Also, they are best used when the flood waves are very similar in shape and magnitude to previous flood waves for which stage and discharge observations are available for calibrating the hydrologic routing parameters (coefficients).

For routing dam-break flood waves, a particular hydraulic method known as the dynamic wave method is chosen. This choice is based on its ability to provide more accuracy in simulating the dam-break flood wave than that provided by the hydrologic methods, as well as other hydraulic methods such as the kinematic wave and diffusion wave methods. Of the many available hydrologic and hydraulic routing techniques, only the dynamic wave method accounts for the acceleration effects associated with the dam-break waves and the influence of downstream unsteady backwater effects produced by channel constrictions, dams, bridge-road embankments, and tributary inflows. Also, the dynamic wave method can be used economically, i.e., the computational costs can be made insignificant if advantages of certain numerical solution techniques are utilized.

The dynamic wave method based on the complete equations of unsteady flow is used to route the dam-break flood hydrograph through the downstream valley. This method is derived from the original equations developed by Barre De Saint-Venant (1871). The only coefficient that must be extrapolated beyond the range of past experience is the coefficient of flow resistance. It so happens that this is usually not a sensitive parameter in effecting the modifications of the flood wave due to its progression through the downstream valley. The applicability of Saint-Venant equations to simulate abrupt waves such as the dam-break wave has been demonstrated by Terzidis and Strelkoff (1970) and by Martin and Zovne (1971) who used a "through computation" method which ignores the presence of shock waves. DAMBRK uses the "through computation" method as opposed to isolating a single shock wave should it occur, and then applying the shock equations to it and using the Saint-Venant equations for all other portions of the flow.

The Saint-Venant unsteady flow equations consist of a conservation of mass equation, i.e.,

$$\frac{\partial Q}{\partial x} + \frac{\partial(A+A_o)}{\partial t} - q = 0 \quad (22)$$

and a conservation of momentum equation, i.e.,

$$\frac{\partial Q}{\partial t} + \frac{\partial(Q^2/A)}{\partial x} + gA\left(\frac{\partial h}{\partial x} + S_f + S_e\right) = 0 \quad (23)$$

where A is the active cross-sectional area of flow, A_o is the inactive (off-channel storage) cross-sectional area, x is the longitudinal distance along the channel (valley), t is the time, q is the lateral inflow or outflow per linear distance along the channel (inflow is positive and outflow is negative in sign), g is the acceleration due to gravity, S_f is the friction slope, and S_e is the expansion-contraction slope. The friction slope is evaluated from Manning's equation for uniform, steady flow, i.e.,

$$S_f = \frac{n^2 |Q| Q}{2.21 A^2 R^{4/3}} \quad (24)$$

in which n is the Manning coefficient of frictional resistance and R is the hydraulic radius defined as A/B where B is the top width of the active cross-sectional area. The term (S_e) is defined as follows:

$$S_e = \frac{k \Delta(Q/A)^2}{2g \Delta x} \quad (25)$$

in which k (Morris and Wiggert, 1972) is the expansion-contraction coefficient varying from 0.0 to ± 1.0 (+ if contraction, - if expansion), and $\Delta(Q/A)^2$ is the difference in the term $(Q/A)^2$ at two adjacent cross-sections separated by a distance Δx .

Eqs. (22)-(23) were modified by the author (Fread, 1975, 1976) and Smith (1978) to better account for the differences in flood wave properties for flow occurring simultaneously in the river channel and the overbank flood plain of the downstream valley. As modified, Eqs. (22)-(23) become:

$$\frac{\partial(K_c Q)}{\partial x_c} + \frac{\partial(K_l Q)}{\partial x_l} + \frac{\partial(K_r Q)}{\partial x_r} + \frac{\partial A}{\partial t} - q = 0 \quad (26)$$

$$\begin{aligned} \frac{\partial Q}{\partial t} + \frac{\partial(K_c^2 Q^2/A_c)}{\partial x_c} + \frac{\partial(K_l^2 Q^2/A_l)}{\partial x_l} + \frac{\partial(K_r^2 Q^2/A_r)}{\partial x_r} + gA_c \left[\frac{\partial h}{\partial x_c} \right. \\ \left. + S_{fc} + S_e \right] + gA_l \left[\frac{\partial h}{\partial x_l} + S_{fl} \right] + gA_r \left[\frac{\partial h}{\partial x_r} + S_{fr} \right] = 0 \end{aligned} \quad (27)$$

in which the subscripts (c), (l), and (r) represent the channel, left flood-plain, and right flood-plain sections, respectively. The parameters (K_c, K_l, K_r) proportion the total flow (Q) into channel flow, left flood-plain flow, and right flood-plain flow, respectively. These are defined as follows:

$$K_c = \frac{1}{1+k_l+k_r} \quad (28)$$

$$K_l = \frac{k_l}{1+k_l+k_r} \quad (29)$$

$$K_r = \frac{k_r}{1+k_l+k_r} \quad (30)$$

in which

$$k_l = \frac{Q_l}{Q_c} = \frac{n_c}{n_l} \frac{A_l}{A_c} \left[\frac{R_l}{R_c} \right]^{2/3} \left[\frac{\Delta x_c}{\Delta x_l} \right]^{1/2} \quad (31)$$

$$k_r = \frac{Q_r}{Q_c} = \frac{n_c A_r}{n_r A_c} \left[\frac{R_r}{R_c} \right]^{2/3} \left[\frac{\Delta x_c}{\Delta x_r} \right]^{1/2} \quad (32)$$

Eqs. (31)-(32) represent the ratio of flow in the channel section to flow in the left and right flood-plain (overbank) sections, where the flows are expressed in terms of the Manning equation in which the energy slope is approximated by the water surface slope ($\Delta h/\Delta x$).

The friction slope terms in Eq. (27) are given by the following:

$$S_{fc} = \frac{n_c^2 |K_c Q| K_c Q}{2.21 A_c^2 R_c^{4/3}} \quad (33)$$

$$S_{fl} = \frac{n_l^2 |K_l Q| K_l Q}{2.21 A_l^2 R_l^{4/3}} \quad (34)$$

$$S_{fr} = \frac{n_r^2 |K_r Q| K_r Q}{2.21 A_r^2 R_r^{4/3}} \quad (35)$$

In Eq. (26), the term A is the total cross-sectional area, i.e.,

$$A = A_c + A_l + A_r + A_o \quad (36)$$

where A_o is the off-channel storage (inactive) area.

Eqs. (22)-(23) and (26)-(27) constitute a system of partial differential equations of the hyperbolic type. They contain two independent variables, x and t, and two dependent variables, h and Q; the remaining terms are either functions of x, t, h, and/or Q, or they are constants. These equations are not amenable to analytical solutions except in cases where the channel geometry and boundary conditions are uncomplicated and the non-linear properties of the equations are either neglected or made linear. The equations may be solved numerically by performing two basic steps. First, the partial differential equations are represented by a corresponding set of finite difference algebraic equations; and second, the system of algebraic equations is solved in conformance with prescribed initial and boundary conditions.

Eqs. (22)-(23) and (26)-(27) can be solved by either explicit or implicit finite difference techniques (Liggett and Cunge, 1975).

Explicit methods, although simpler in application, are restricted by mathematical stability considerations to very small computational time steps (on the order of a few minutes or even seconds). Such small time steps cause the explicit methods to be very inefficient in the use of computer time. Implicit finite difference techniques (Preissmann, 1961; Amein and Fang, 1970; Strelkoff, 1970), however, have no restrictions on the size of the time step due to mathematical stability; however, convergence considerations may require its size to be limited (Fread, 1974a).

Of the various implicit schemes that have been developed, the "weighted four-point" scheme first used by Preissmann (1961), and more recently by Chaudhry and Contractor (1973) and Fread (1974b, 1978), appears most advantageous since it can readily be used with unequal distance steps and its stability-convergence properties can be easily controlled. In the weighted four-point implicit finite difference scheme, the continuous x-t region in which solutions of h and Q are sought, is represented by a rectangular net of discrete points. The net points are determined by the intersection of lines drawn parallel to the x and t axes. Those parallel to the x axis represent time lines; they have a spacing of Δt , which need not be constant. Those parallel to the t axis represent discrete locations or nodes along the river (x axis); they have a spacing of Δx , which also need not be constant. Each point in the rectangular network can be identified by a subscript (i) which designates the x position and a superscript (j) which designates the time line.

The time derivatives are approximated by a forward difference quotient centered between the i^{th} and $i+1$ points along the x axis, i.e.,

$$\frac{\partial K}{\partial t} \approx \frac{K_i^{j+1} + K_{i+1}^{j+1} - K_i^j - K_{i+1}^j}{2 \Delta t_j} \quad (37)$$

where K represents any variable.

The spatial derivatives are approximated by a forward difference quotient positioned between two adjacent time lines according to weighting factors of θ and $1-\theta$, i.e.,

$$\frac{\partial K}{\partial x} \approx \theta \left[\frac{K_{i+1}^{j+1} - K_i^{j+1}}{\Delta x_i} \right] + (1-\theta) \left[\frac{K_{i+1}^j - K_i^j}{\Delta x_i} \right] \quad (38)$$

Variables other than derivatives are approximated at the time level where the spatial derivatives are evaluated by using the same weighting factors, i.e.,

$$K = \theta \left[\frac{K_i^{j+1} + K_{i+1}^{j+1}}{2} \right] + (1-\theta) \left[\frac{K_i^j + K_{i+1}^j}{2} \right] \quad (39)$$

A θ weighting factor of 1.0 yields the fully implicit or backward difference scheme used by Baltzer and Lai (1968). A weighting factor of 0.5 yields the box scheme used by Amein and Fang (1970). The influence of the θ weighting factor on the accuracy of the computations was examined by Fread (1974a), who concluded that the accuracy decreases as θ departs from 0.5 and approaches 1.0. This effect becomes more pronounced as the magnitude of the computational time step increases. Usually, a weighting factor of 0.60 is used so as to minimize the loss of accuracy associated with greater values while avoiding the possibility of a weak or pseudo instability noticed by Baltzer and Lai (1968), and Chaudhry and Contractor (1973); however, θ may be specified other than 0.60 in the data input to the DAMBRK model.

When the finite difference operators defined by Eqs. (37)-(39) are used to replace the derivatives and other variables in Eqs. (22)-(23), the following weighted four-point implicit difference equations are obtained:

$$\theta \left[\frac{Q_{i+1}^{j+1} - Q_i^{j+1}}{\Delta x_i} \right] - \theta q_i^{j+1} + (1-\theta) \left[\frac{Q_{i+1}^j - Q_i^j}{\Delta x_i} \right] - (1-\theta) q_i^j + \left[\frac{(A+A_o)_i^{j+1} + (A+A_o)_{i+1}^{j+1} - (A+A_o)_i^j - (A+A_o)_{i+1}^j}{2\Delta t_j} \right] = 0 \quad (40)$$

$$\left(\frac{Q_i^{j+1} + Q_{i+1}^{j+1} - Q_i^j - Q_{i+1}^j}{2\Delta t_j} \right) + \theta \left[\frac{(Q^2/A)_{i+1}^{j+1} - (Q^2/A)_i^{j+1}}{\Delta x_i} + g \bar{A}^{j+1} \right] + (1-\theta) \left[\frac{(Q^2/A)_{i+1}^j - (Q^2/A)_i^j}{\Delta x_i} + g \bar{A}^j \left(\frac{h_{i+1}^j - h_i^j}{\Delta x_i} + \bar{s}_f^j + s_{ce}^j \right) \right] = 0 \quad (41)$$

where:

$$\bar{A} = (A_i + A_{i+1})/2 \quad (42)$$

$$\bar{S}_f = n^2 \bar{Q} |\bar{Q}| / (2.2 \bar{A}^2 \bar{R}^{4/3}) \quad (43)$$

$$\bar{Q} = (Q_i + Q_{i+1})/2 \quad (44)$$

$$\bar{R} = \bar{A}/\bar{B} \quad (45)$$

$$\bar{B} = (B_i + B_{i+1})/2 \quad (46)$$

The terms associated with the j^{th} time line are known from either the initial conditions or previous computations. The initial conditions refer to values of h and Q at each node along the x axis for the first time line ($j=1$).

Eqs. (40)-(41) cannot be solved in an explicit or direct manner for the unknowns since there are four unknowns and only two equations. However, if Eqs. (40)-(41) are applied to each of the $(N-1)$ rectangular grids between the upstream and downstream boundaries, a total of $(2N-2)$ equations with $2N$ unknowns can be formulated. (N denotes the total number of nodes). Then, prescribed boundary conditions, one at the upstream boundary and one at the downstream boundary, provide the necessary two additional equations required for the system to be determinate. The resulting system of $2N$ non-linear equations with $2N$ unknowns is solved by a functional iterative procedure, the Newton-Raphson method (Amein and Fang, 1970).

Computations for the iterative solution of the non-linear system are begun by assigning trial values to the $2N$ unknowns. Substitution of the trial values into the system of non-linear equations yields a set of $2N$ residuals. The Newton-Raphson method provides a means for correcting the trial values until the residuals are reduced to a suitable tolerance level. This is usually accomplished in one or two iterations through use of linear extrapolation for the first trial values. If the Newton-Raphson corrections are applied only once, i.e., there is no iteration, the non-linear system of difference equations degenerates to the equivalent of a quasi-linear formulation which may require smaller time steps than the non-linear formulation for the same degree of numerical accuracy.

A system of $2N \times 2N$ linear equations relates the corrections to the residuals and to a Jacobian coefficient matrix composed of partial derivatives of each equation with respect to each unknown variable in that equation. The coefficient matrix of the linear system has a banded structure which allows the system to be solved by a compact quad-diagonal Gaussian elimination algorithm (Fread, 1971), which is very efficient with respect to computing time and storage. The required storage is $2N \times 4$ and the required number of computational steps is approximately $38N$.

The DAMBRK model has the option to use either Eqs. (22)-(23) or Eqs. (26)-(27). The former is a somewhat simpler treatment in which a total or composite cross-section is used, whereas the latter set utilizes a more detailed representation of the flow cross-section. Eqs. (26)-(27) are recommended when the channel is sufficiently large to carry a significant portion of the total flow and the channel has a rather meandering path through the downstream valley.

2.4 Initial and Boundary Conditions

In order to solve the unsteady flow equations the state of the flow (h and Q) must be known at all cross-sections at the beginning (t=0) of the simulation. This is known as the initial condition of the flow. The DAMBRK model assumes the flow to be steady, non-uniform flow where the flow at each cross-section is initially computed to be:

$$Q_i = Q_{i-1} + q_{i-1} \Delta x_{i-1} \quad i=2,3,\dots,N \quad (47)$$

where Q_1 is the known steady discharge at the dam, i.e., the upstream boundary of the downstream valley, and q_i is any lateral inflow from tributaries existing between the cross-sections spaced at intervals of Δx along the valley. The steady discharge from the dam at t=0 must be non-zero, i.e., a dry downstream channel is not amenable to simulation by DAMBRK. This is not an important restriction, especially when maximum flows and peak stages are of paramount interest in the dam-break flood. The tributary lateral inflow must be specified by the forecaster throughout the simulation period. If these flows are relatively small, they may be safely ignored.

The water surface elevations associated with the steady flow must also be computed at t=0. This is accomplished by solving the following equation:

$$\frac{(Q^2/A)_{i+1} - (Q^2/A)_i}{\Delta x_i} + g \left[\frac{A_i + A_{i+1}}{2} \right] \left[\frac{h_{i+1} - h_i}{\Delta x_i} + \frac{n^2 (Q_i + Q_{i+1})^2 (B_i + B_{i+1})^{4/3}}{2.2 (A_i + A_{i+1})^{10/3}} \right] = 0 \quad (48)$$

This equation may be easily solved using the Newton-Raphson method by starting at a specified elevation at the downstream extremity of the valley and solving for the adjacent upstream elevation step by step until the upstream boundary is reached. The downstream specified elevation may be obtained from a solution of the Manning equation if the flow is governed only by the channel conditions; however, if

a flow control structure produces a back-up of the flow at this location, the forecaster must directly specify the water surface elevation existing at the downstream boundary at $t=0$.

In addition to initial conditions, boundary conditions at the upstream and downstream sections of the valley must be specified for all times ($t=0$ to $t=t_e$ where t_e is the future time at which the simulation ceases).

At the upstream boundary the reservoir outflow hydrograph $Q(t)$ provides the necessary boundary condition.

At the downstream boundary an appropriate stage-discharge relation is used. If the flow at the downstream extremity is channel-controlled, the following relation is used:

$$Q_N = \frac{1.49}{n} A_N^{5/3} / B_N^{2/3} \left[\frac{h_{N-1} - h_N}{\Delta x_{N-1}} \right]^{1/2} \quad (49)$$

Eq. (49) reproduces the hysteresis effect in stage-discharge relations often observed as a loop-rating curve. The loop (hysteresis) is produced by the temporal variations in the water surface slope. If the flow at the downstream boundary is controlled by a flow control structure such as a dam, the following relation is used:

$$Q_N = Q_b + Q_s \quad (50)$$

where the breach flow (Q_b) is defined by Eq. (2) and the spillway flow (Q_s) is defined by Eq. (17) in which the various terms apply to the dam at the downstream boundary. Since the resulting expressions for Q_b and Q_s are in terms of the water surface elevation h_N , Eq. (50) is a stage-discharge relation.

The downstream boundary condition may also be specified as a single-value rating curve in which the stage-discharge values are input as tabular values. Linear interpolation is used for determining intermediate values.

2.5 Multiple Dams and Bridges

The DAMBRK model can simulate the progression of a dam-break wave through a downstream valley containing a reservoir created by another downstream dam, which itself may fail due to being sufficiently overtopped by the wave produced by the failure of the upstream dam. In fact, an unlimited number of reservoirs located sequentially along the valley can be simulated. In DAMBRK there is a choice of two methods for simulating dam-break flows in a valley having multiple dams.

In the first method, which is known as the "sequential method," the downstream boundary condition for the dynamic routing component is given by Eq. (50) rather than Eq. (49). The properties of the downstream dam, spillways, breach description, and elevation of flow which precipitates the failure of the dam, are used in Eq. (50). In this way, backwater effects of the downstream dam are included in the routing of the outflow hydrograph from the upstream dam. The most upstream reservoir may be simulated using either storage or dynamic routing.

When the tailwater below a dam is affected by flow conditions downstream of the tailwater section (e.g., backwater produced by a downstream dam, flow constriction, bridge, and/or tributary inflow), the flow occurring at the dam is computed by the second method known as the "simultaneous method" which uses an internal boundary condition at the dam. In this method the dam is treated as a short Δx reach in which the flow through the reach is governed by the following two equations rather than either Eqs. (22)-(23) or Eqs. (26)-(27):

$$Q_i = Q_{i+1} \quad (51)$$

$$Q_i = Q_b + Q_s \quad (52)$$

in which Q_b and Q_s are breach flow and spillway flow as described in Eqs. (2) and (17). In this way the flows, Q_i and Q_{i+1} , and the elevations, h_i and h_{i+1} , are in balance with the other flows and elevations occurring simultaneously throughout the entire flow system; the system may consist of additional dams which are treated as additional internal boundary conditions via Eqs. (51)-(52). The "simultaneous method" requires dynamic routing to be used in the most upstream reservoir. This method can also be used for a flow system having a single dam, only.

Highway/railway bridges and their associated earthen embankments which are located at points downstream of a dam may also be treated as internal boundary conditions. Eqs. (51)-(52) are used at each bridge; the term Q_s in Eq. (52) is computed by the following expression:

$$Q_s = 8.02 C A_{i+1} (h_i - h_{i+1})^{1/2} + c_{cu} L_u k_u (h_i - h_{cu})^{3/2} + c_{cl} L_l k_l (h_i - h_{cl})^{3/2} \quad (53)$$

in which

$$k_u = 1.0 \quad \text{if} \quad h_{ru} \leq 0.76 \quad (54)$$

$$k_u = 1.0 - c_u (h_{ru} - 0.76)^3 \quad \text{if} \quad h_{ru} > 0.76 \quad (55)$$

$$c_u = 133(h_{ru} - 0.78) + 1 \quad \text{if} \quad 0.76 \leq h_{ru} \leq 0.96 \quad (56)$$

$$c_u = 400(h_{ru} - 0.78) + 10 \quad \text{if} \quad h_{ru} > 0.96 \quad (57)$$

$$h_{ru} = (h_{i+1} - h_{cu}) / (h_i - h_{cu}) \quad (58)$$

$$cc_u = 3.02(h_i - h_{cu})^{0.05} \quad \text{if} \quad 0 < h_u \leq 0.15 \quad (59)$$

$$cc_u = 3.06 + 0.27(h_u - 0.15) \quad \text{if} \quad h_u > 0.15 \quad (60)$$

$$h_u = (h_i - h_{cu}) / w_u \quad (61)$$

in which C is a coefficient of bridge flow (see Chow, 1959), A_{i+1} is the cross-section flow area of the bridge opening at section $i+1$ (downstream end of bridge), h_{cu} is the elevation of the upper embankment crest, h_i is the water surface elevation at section i (upstream end of bridge), h_{i+1} is the water surface elevation at section $i+1$, L_u is the length of the upper embankment crest perpendicular to flow direction), k_u is the submergence correction factor for flow over the upper embankment crest, and w_u is the width (parallel to flow direction) of the crest of the upper embankment. In Eq. (53) the terms with an (l) subscript refer to a lower embankment crest and these terms are defined by Eqs. (54)-(61) in which the (u) subscripts are replaced with (l) subscripts. Eqs. (54)-(61) were developed from basic information on flow over road embankments as reported by the U.S. Dept. of Transportation (1978).

2.6 Supercritical Flow

The DAMBRK model can simulate the flow through the downstream valley when the flow is supercritical. This type of flow occurs when the slope of the downstream valley exceeds about 50 ft/mi. Slopes less than this usually result in the flow being subcritical to which all preceding comments pertaining to the downstream routing apply. When the flow is supercritical, any flow disturbances cannot travel back upstream; therefore, the downstream boundary becomes superfluous. Thus, for supercritical flow, a downstream boundary condition is not required; however, another equation in addition to the reservoir outflow hydrograph is needed for the upstream boundary condition. To satisfy this requirement, an equation similar to Eq. (49) is used at the upstream boundary, i.e.,

$$Q_1 = \frac{1.486}{n} A_1^{5/3} / B_1^{5/3} \left[\frac{h_1 - h_2}{\Delta x_1} \right]^{1/2} \quad (62)$$

A modified compact quad-diagonal Gaussian elimination algorithm similar to the one previously described is required for solving the unsteady flow equations when supercritical flow exists. The modification results when the form of the Jacobian coefficient matrix is slightly changed due the need for two upstream boundary conditions and none at the downstream boundary.

The DAMBRK model is constructed to accommodate supercritical flow for either the entire channel reach or for only an upstream portion of the entire reach. The supercritical flow regime is assumed to be applicable throughout the duration of the flow. Multiple reservoirs on supercritical valley slopes must be treated using a storage routing technique such as Eq. (18) rather than the dynamic routing technique.

2.7 Routing Losses

Often in the case of dam-break floods, where the extremely high flows inundate considerable portions of channel overbank or valley flood plain, a measurable loss of flow volume occurs. This is due to infiltration into the relatively dry overbank material, detention storage losses, and sometimes short-circuiting of flows from the main valley into other drainage basins via canals or overtopping natural ridges separating the drainage basins. Such losses of flow may be taken into account via the term q in Eq. (22) or Eq. (26). An expression describing the loss is given by the following:

$$q_m = -0.00458 V_L P / (L \bar{T}) \quad (63)$$

in which V_L is the outflow volume (acre-ft) from the reservoir; P is the volume loss ratio; L is the length (mi) of downstream channel through which the loss occurs; and T is the average duration (hr) of the flood wave throughout the reach length L ; and q_m is the maximum lateral outflow (cfs/ft) occurring along the reach L throughout the duration of flow. The mean lateral outflow is proportioned in time and distance along the reach L such that $q_i^j = 0$ when $Q_i^j = Q_i^1$ and $q_i^j = q_m$ when $q_i^j = Q_{\max_i}$. Thus:

$$q_i^j = \frac{(Q_i^j - Q_i^1)}{(Q_{\max_i} - Q_i^1)} q_m \quad (64)$$

where Q_i^1 is the initial flow and Q_{\max_i} is the estimated maximum flow at each node determined a priori according to an exponential attenuation of the peak flow at the dam. The parameter P may vary from only a few percent to more than 30, depending on the conditions of the downstream valley.

2.8 Tributary Inflows

Unsteady flows from tributaries downstream of the dam can be added to the unsteady flow resulting from the dam failure. This is accomplished via the term q in Eq. (22) or Eq. (26). The tributary flow is distributed along a single Δx reach. Backwater effects of the dam-break flow on the tributary flow are ignored, and the tributary flow is assumed to enter perpendicular to the dam-break flow.

2.9 Reservoir Dynamic Routing

As mentioned earlier, an option is provided in the DAMBRK model to use dynamic routing rather than storage routing to compute the reservoir outflow hydrograph. The dynamic routing is identical to the above description with the exception of boundary conditions. The upstream boundary condition is a discharge hydrograph given by the following:

$$Q_1^{j+1} - I(t) = 0 \quad (65)$$

where $I(t)$ is the known reservoir inflow hydrograph. The downstream boundary condition is a stage-discharge relation given by Eq. (50). The initial water surface elevations are computed by solving Eq. (48), the steady gradually varied backwater equation, using h_0 which is the elevation of the water surface at the dam site when the computation commences. The reservoir dynamic routing procedure must contend with the lowering of the water surface elevation at the upstream boundary as the reservoir volume is depleted by the outflow through the breach. If this depth becomes small and approaches a value less than the normal depth, the computations become unstable. To avoid this computational problem, the upstream depth is constantly monitored; if it becomes less than the initial normal depth (d_n), the location of the upstream boundary condition is shifted downstream one node at a time until the depth at the node is greater than d_n .

2.10 Landslide-Generated Waves

Reservoirs are sometimes subject to landslides which rush into the reservoir, displacing a portion of the reservoir contents and, thereby, creating a very steep water wave which travels up and down the length of the reservoir (Davidson and McCartney, 1975). This wave may have sufficient amplitude to overtop the dam and precipitate a failure of the dam, or the wave by itself may be large enough to cause catastrophic flooding downstream of the dam without resulting in the failure of the dam as perhaps in the case of a concrete dam such as the Viant Dam flood of 1963.

The capability to generate waves produced by landslides is provided within DAMBRK. The volume of the landslide mass, its porosity, and time

interval over which the landslide occurs, are input to the model. In the model, the landslide mass is deposited within the reservoir in layers during small computational time steps, and simultaneously the original dimensions of the reservoir are reduced accordingly. The time rate of reduction in the reservoir cross-sectional area (Koutitas, 1977) creates the wave during the solution of the unsteady flow, Eqs. (22)-(23), which are applied to the cross-sections describing the reservoir characteristics. The upstream boundary condition is given by Eq. (65), and the downstream boundary condition is given by Eq. (50). The initial conditions are obtained as described by Eqs. (47)-(48) for steady non-uniform flow.

Wave runup is not considered in the model. For near vertical faces of concrete dams the runup may be neglected; however, for earthen dams the angle of the earth fill on the reservoir side will result in a surge which will advance up the face of the dam to a height approximately equal to 2.5 times the height of the landslide-generated wave (Morris and Wiggert, 1972).

2.11 Selection of Δt and Δx

Rapidly rising hydrographs, such as the dam-break outflow hydrograph, can cause computational problems (instability and non-convergence) when applied to numerical approximations of the unsteady flow equations. This is the case even when an implicit, non-linear finite difference solution technique is used. However, many computational problems can be overcome by proper selection of time step (Δt) size and the distance step (Δx) size. During the limited testing of the model presented herein, two types of computational problems arose. First, if the time step were too large relative to the rate of increase of discharge during that time step, errors occurred in the computed water surface elevation in the vicinity of the wave front. These water surface elevations would tend to dip toward the channel bottom and quickly cause negative areas to be computed which would then cause the computations to "blow up." Second, too large a time step would also cause the Newton-Raphson iteration to not converge. The first computational problem is similar to that experienced by Cunge (1975). Both of the computational problems were successfully treated by reducing the time step size by a factor of 0.5 whenever negative areas were computed, or when a reasonable number of iterations were exceeded. With the reduced time step, the computations were repeated. If the same problems persisted, the time step was again halved and the computations repeated. Usually, one or two reductions would be sufficient. The computational process was then advanced to the next time level by the original unreduced time step. Computations were initially begun with Δt time steps (hr) computed via the following relations:

$$\Delta t = 0.5 \qquad t \leq t_b - 0.5 \qquad (66)$$

$$\Delta t = \tau/20 \qquad t_b - 0.5 < t < t_b + 2\tau \qquad (67)$$

in which τ is the time (hr) to peak of the outflow hydrograph and t_b is the time (hr) at which the breach starts to form.

Distance steps (Δx) are selected in the following range:

$$\Delta x \approx c \Delta t \quad (68)$$

where c is the wave speed in mi/hr and Δx is in miles. The dam-break hydrograph tends to be a very peaked-type of hydrograph and, as such, tends to dampen and flatten out as it advances downstream. Accordingly, the time step may be increased as the wave progresses downstream; therefore, smaller values of Δx are selected immediately downstream of the dam, with a gradual increase in size at greater distances downstream of the dam. Also, the smaller values of Δx are associated with the smaller values of τ . This methodology of selecting Δx and Δt values follows the guidelines set forth in an analysis made by Fread (1974a) of the numerical properties of the four-point implicit solution of the unsteady flow equations.

Since the flood wave dampens out as it moves downstream, the Δt time step may be increased as the computations advance in time. The following scheme is used:

$$\Delta t = T_p / 20 \quad t \geq t_b + 2\tau \quad (69)$$

where T_p is the time between the start of rise of the hydrograph and the peak of the hydrograph at selected locations along the downstream valley. Six evenly spaced locations along the downstream valley commencing at the dam site are monitored to determine T_p . The peak must have occurred at one of the locations before T_p can be evaluated. Since T_p increases at locations farther and farther downstream of the dam, the T_p which exists for the most downstream location is used in Eq. (69). A Δt determined by the division of T_p into twenty parts is considered appropriate to maintain an adequate level of numerical accuracy. An option exists to maintain throughout the computations the time step size specified in the data input. The units of Δt , t_b , and T_p are hours.

3. DATA REQUIREMENTS

The DAMBRK model was developed so as to require data that was accessible to the forecaster. The input data requirements are flexible insofar as much of the data may be ignored (left blank on the input data cards or omitted altogether) when a detailed analysis of a dam-break flood inundation event is not feasible due to lack of data or insufficient data preparation time. Nonetheless, the resulting approximate analysis is more accurate and convenient to obtain than that which could be computed by other techniques. The input data can be categorized into two groups.

The first data group pertains to the dam (the breach, spillways, and reservoir storage volume). The breach data consists of the following parameters: τ (failure time of breach, in hours); b (final bottom width of breach); z (side slope of breach); h_{bm} (final elevation of breach bottom); h_0 (initial elevation of water in reservoir); h_f (elevation of water when breach begins to form); and h_d (elevation of top of dam). The spillway data consists of the following: h_s (elevation of uncontrolled spillway crest); c_s (coefficient of discharge of uncontrolled spillway); h_g (elevation of center of submerged gated spillway); c_g (coefficient of discharge of gated spillway); c_d (coefficient of discharge of crest of dam); and Q_t (constant, head independent discharge from dam). The storage parameters consist of the following: a table of surface area (A_s) in acres or volume in acre-ft. and the corresponding elevations within the reservoir. The forecaster must estimate the values of τ , b , z , h_{bm} , and h_f . The remaining values are obtained from the physical description of the dam, spillways, and reservoir. In some cases h_s , c_s , h_g , c_g , and c_d may be ignored and Q_t used in their place.

The second group pertains to the routing of the outflow hydrograph through the downstream valley. This consists of a description of the cross-sections, hydraulic resistance coefficients, and expansion coefficients. The cross-sections are specified by location mileage, and tables of top width (active and inactive) and corresponding elevations. The active top widths may be total widths as for a composite section, or they may be left flood-plain, right flood-plain, and channel widths. The top widths can be obtained from USGS topography maps, 7 1/2' series, scale 1:24000. The channel widths are usually not as significant for an accurate analysis as the overbank widths (the latter are available from the topo maps). The number of cross-sections used to describe the downstream valley depends on the variability of the valley widths. A minimum of two must be used. Additional cross-sections are created by the model via linear interpolation between adjacent cross-sections specified by the forecaster. This feature enables only a minimum of cross-sectional data to be input by the forecaster according to such criteria as data availability, variation, preparation time, etc. The number of interpolated cross-sections created by the model is controlled by the parameter DXM which is input for each reach between specified cross-sections. The hydraulic resistance coefficients consist of a table of Manning's n vs. elevation for each reach between specified cross-sections. The expansion-contraction coefficients (k) are specified as non-zero values at sections where significant expansion or contractions occur. The k parameters may be left blank in most analyses.

4. MODEL TESTING

The DAMBRK model has been tested on five historical dam-break floods to determine its ability to reconstitute observed downstream peak stages, discharges, and travel times. Those floods that have

been used in the testing are: 1976 Teton Dam, 1972 Buffalo Creek Coal-Waste Dam, 1889 Johnstown Dam, 1977 Toccoa (Kelly Barnes) Dam, and the 1977 Laurel Run Dam floods. However, only the Teton and Buffalo Creek floods will be presented herein.

4.1 Teton Dam Flood

The Teton Dam, a 300 ft. high earthen dam with a 3,000 ft. long crest and 250,000 acre-ft of stored water, failed on June 5, 1976, killing 11 people, making 25,000 homeless, and inflicting about \$400 million in damages to the downstream Teton-Snake River Valley. Data from a Geological Survey Report by Ray, et al. (1977) provided observations on the approximate development of the breach, description of the reservoir storage, downstream cross-sections and estimates of Manning's n approximately every 5 miles, indirect peak discharge measurements at 3 sites, flood-peak travel times, and flood-peak elevations. The inundated area is shown in Fig. 2.

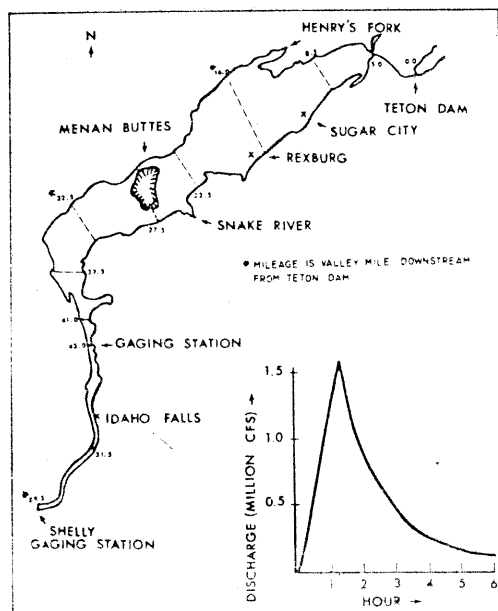


Fig. 2 - OUTFLOW HYDROGRAPH AND FLOODED AREA DOWNSTREAM OF TETON DAM

The following breach parameters were used in DAMBRK to reconstitute the downstream flooding due to the failure of Teton Dam: $\tau = 1.25$ hrs., $b = 150$ ft., $z = 0$, $h_{bm} = 0.0$, $h_f = h_d = h_o = 261.5$ ft. Cross-sectional properties at 12 locations shown in Fig. 2 along the 60-mile reach of the Teton-Snake River Valley below the dam were used. Five top widths were used to describe each cross-section. The downstream valley consisted of a narrow canyon (approx. 1,000 ft. wide) for the first 5 miles and thereafter a wide valley which was inundated to a width of about 9 miles. Manning's n values ranging from 0.028 to 0.047 were provided from field estimates by the Geological Survey. DXM values

between cross-sections were assigned values that gradually increased from 0.5 miles near the dam, to a value of 1.5 miles near the downstream boundary at the Shelly gaging station (valley mile 59.5 downstream from the dam). The reservoir surface area-elevation values were obtained from Geological Survey topo maps. The downstream boundary was assumed to be channel flow control as represented by a loop rating curve given by Eq. (49).

The computed outflow hydrograph is shown in Fig. 2. It has a peak value of 1,652,300 cfs (cubic feet per second), a time to peak of 1.25 hrs., and a total duration of about 6 hours. This peak discharge is about 20 times greater than the flood of record at Idaho Falls. The temporal variation of the computed outflow volume compared within 5 percent of observed values as shown in Fig. 3. In Fig. 4 a comparison is presented of Teton reservoir outflow hydrographs

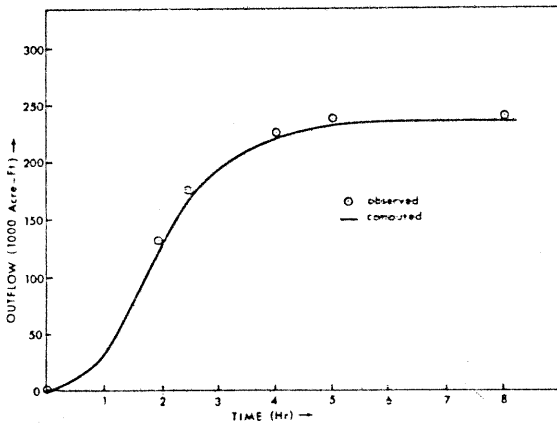


Fig. 3 - OUTFLOW VOLUME FROM TETON DAM

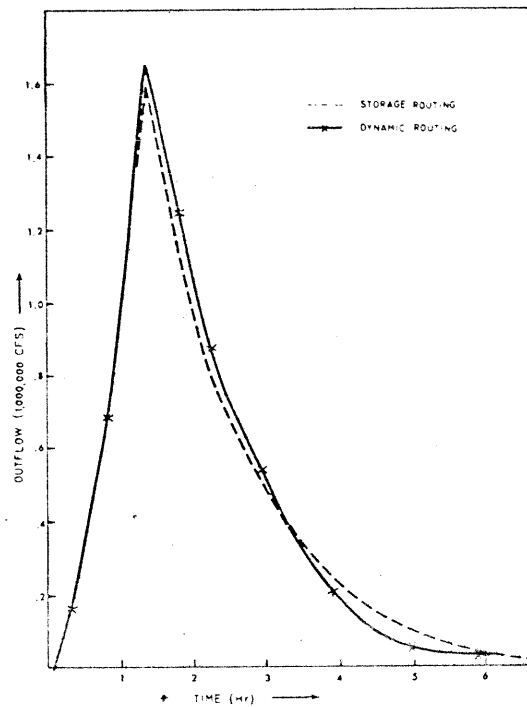


Fig. 4 - OUTFLOW HYDROGRAPH FROM TETON DAM FAILURE

computed via reservoir storage routing and reservoir dynamic routing. Since the breach of the Teton Dam formed gradually over approximately a one-hour interval, a steep negative wave did not develop. Also, the inflow to the reservoir was not very significant. For these two reasons, the reservoir surface remained essentially level during the reservoir drawdown and the dynamic routing yielded almost the same outflow hydrograph as the level pool, storage routing technique.

The computed peak discharge values along the 60-mile downstream valley are shown in Fig. 5 along with three observed (indirect measurement) values at miles 8.5, 43.0, and 59.5. The average difference between the computed and observed values is 4.8 percent. Most apparent is the extreme attenuation of the peak discharge as the flood wave progresses through the valley. Two computed curves are shown in Fig. 5; one in which no losses were assumed, i.e., $q_m = 0$; and a second in which the losses were assumed to vary from zero to a maximum of $q_m = -0.30$ cfs/ft and were accounted for in the model through the q term in Eq. (22). Losses were due to infiltration and detention storage behind irrigation levees amounting to about 25 percent of the reservoir outflow volume. Eq. (63) was used to compute q_m .

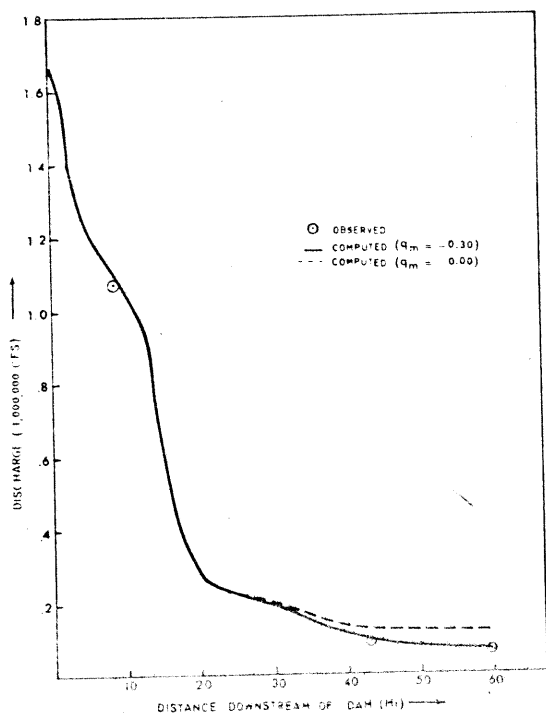


Fig 5 - PROFILE OF PEAK DISCHARGE FROM TETON DAM FAILURE

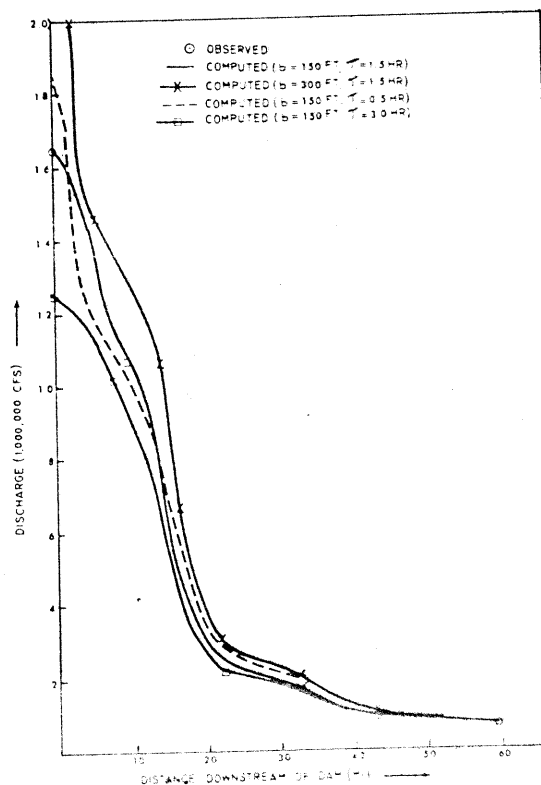


Fig. 6--PROFILE OF PEAK DISCHARGE FROM TETON DAM FAILURE SHOWING SENSITIVITY OF VARIOUS INPUT PARAMETERS

The a priori selection of the breach parameters (τ and b) causes the greatest uncertainty in forecasting dam-break flood waves. The sensitivity of downstream peak discharges to reasonable variations in τ and b are shown in Fig. 6. Although there are large differences in the discharges (+45 to -25 percent) near the dam, these rapidly diminish in the downstream direction. After 10 miles the variation is +20 to -14 percent, and after 15 miles the variation has further diminished (+15 to -8 percent). The tendency for extreme peak

attenuation and rapid damping of differences in the peak discharge is accentuated in the case of Teton Dam due to the presence of the very wide valley. Had the narrow canyon extended all along the 60-mile reach to Shelly, the peak discharge would not have attenuated as much and the differences in peak discharges due to variations in τ and \bar{b} would be more persistent. In this instance, the peak discharge would have attenuated to about 350,000 rather than 67,000 as shown in Fig. 6, and the differences in peak discharges at mile 59.5 would have been about 27 percent as opposed to less than 5 percent as shown in Fig. 6.

Computed peak elevations compared favorably with observed values, as shown in Fig. 7. The average absolute error was 1.5 ft., while the average arithmetic error was only -0.2 ft.

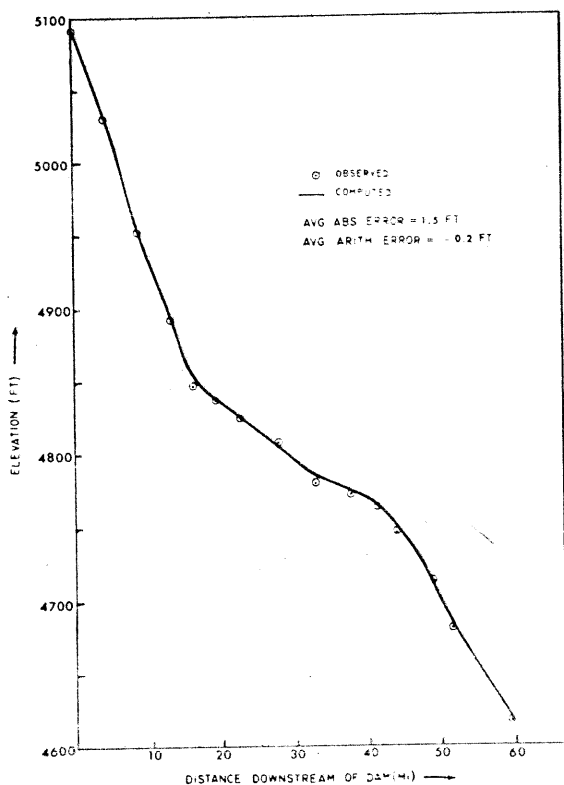


Fig. 7 - PROFILE OF PEAK FLOOD ELEVATION FROM TETON DAM FAILURE

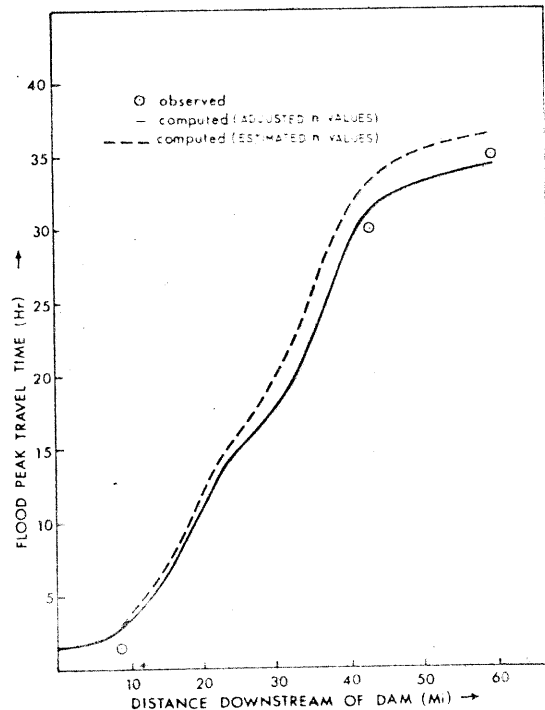


Fig. 8 - TRAVEL TIME OF FLOOD PEAK FROM TETON DAM FAILURE

The computed flood-peak travel times and three observed values are shown in Fig. 8. The differences between the computed and observed are about 10 percent for the case of using the estimated Manning's n values and about 1 percent if the n values are slightly increased by 7 percent.

As mentioned previously, the Manning's n must be estimated, especially for the flows above the flood of record. The sensitivity

of the computed stages and discharges of the Teton flood due to a substantial change (20 percent) in the Manning's n was found to be as follows: 1) 0.5 ft in computed peak water surface elevations or about 2 percent of the maximum flow depths, 2) 16 percent deviation in the computed peak discharges, 3) 0.8 percent change in the total attenuation of peak discharge incurred in the 60-mile reach from Teton Dam to Shelly, and 4) 15 percent change in the flood-peak travel time at Shelly. These results indicate that Manning's n has little effect on peak elevations or depths; however, the travel time is affected by nearly the same percent that the n values are changed.

A typical simulation of the Teton flood as described above involved 78 Δx reaches, 55 hrs. of prototype time, and an initial time step (Δt) of 0.06 hrs. Such a simulation run required only 19 seconds of CPU time on an IBM 360/195 computer system; the associated cost was less than \$5 per run.

4.2 Buffalo Creek Flood

The DAMBRK model was also applied to the failure of the Buffalo Creek coal-waste dam which collapsed on the Middle Fork, a tributary of Buffalo Creek (see Fig. 9) in southwestern West Virginia near Saunders. The dam failed very rapidly on February 26, 1972, and

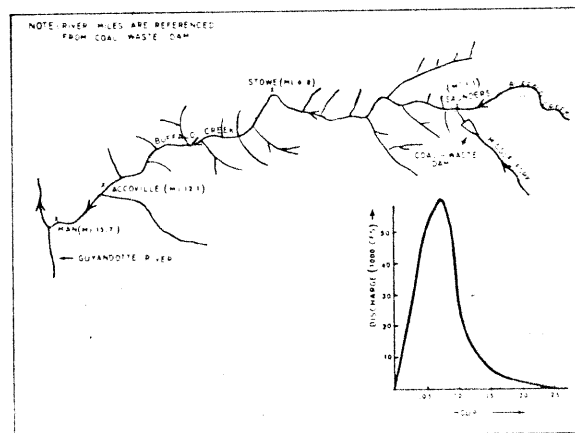


Fig 9 - OUTFLOW HYDROGRAPH FROM COAL-WASTE DAM AND LOCATION PLAN OF BUFFALO CREEK

released about 500 acre-feet of impounded waters into Buffalo Creek valley, causing the most catastrophic flood in the state's history with the loss of 118 lives, 500 homes, and property damage exceeding \$50 million. Observations were available on the approximate development sequence of the breach, the time required to empty the reservoir, indirect peak discharge measurements at four sites, approximate flood-peak travel times, and flood-peak elevations (Davies, et al., 1972). Cross-sections and estimates of the Manning roughness coefficients were taken from a report on routing dam-break floods by McQuivey and Keefer (1975).

The time of failure was estimated to be in the range of 5 minutes and the reservoir took only 15 minutes to empty according to eyewitness reports. The following breach parameters were used: $\tau = 0.083$ hours; $b = 170$ feet, $z = 2.6$ feet, $h_{bm} = 0.0$ feet, $h_f = h_d = h_o = 40.0$ feet. Cross-sectional properties were specified for eight locations along the 15.7 mile reach from the coal-waste dam to below Man at the confluence of Buffalo Creek with the Guyandotte River as shown in Fig. 9. The downstream valley widened from the narrow width (approximately 100 ft) of Middle Fork to about 400-600 feet width of Buffalo Creek Valley. Minimum Δx (D_{xm}) values were gradually increased from 0.2 mile near the dam to 0.4 mile near Man at the downstream boundary. The reservoir area-elevation values were obtained from Davies, et al., (1972).

The 15.7 mile reach was divided into two reaches; one was approximately 4 miles long, in which the very steep channel bottom slope (84 ft/mi) produced supercritical flows, and the second extended on downstream approximately 12 miles, with an average bottom slope of 40 ft/mi, in which subcritical flow prevailed. The computations were unstable when the supercritical reach was modeled using the same type of boundary conditions as used with subcritical flows. This computational problem was eliminated when the supercritical boundary condition, Eq. (62), was used.

The reservoir storage routing option was used to generate the outflow hydrograph shown in Fig. 9. The computations indicated the reservoir was drained of its contents in approximately 15 minutes, which agreed with the observed time to completely empty its contents. The indirect measurements of peak discharge at miles 1.1, 6.8, 12.1, and 15.7 downstream of the dam are shown in Fig. 10. Again, as in the Teton Dam flood, the flood peak was greatly attenuated as it advanced downstream. Whereas the Teton flood was attenuated by a factor of 0.69 in the first 16 miles of which 11 miles included the wide, flat valley below the Teton Canyon, the Buffalo Creek flood was confined to a relatively narrow valley, but was attenuated by a factor of 0.88 in the same distance. The attenuation of the Buffalo Creek flood was due to the much smaller volume of its outflow hydrograph compared with that of the Teton flood.

In Fig. 10, the computed discharges agree favorably with the observed. There are two curves of the computed peak discharge in Fig. 10; one is associated with n values of 0.040. In the former, the n values are representative of field estimates, while the latter results from adjustments in the n values such that computed flood travel times compare favorably with the observed. (Comparison of computed flood travel times with the observed are shown in Fig. 11 for estimated n values and for the final adjusted n values.) It should be noted that the two computed curves in Fig. 10 are not significantly different, although the n values differ by a factor of 1.75. Again, as in the Teton application, the n values influence the time of travel much more than the peak discharge. The large adjusted n values appear

to be appropriate for dam-break waves in the near vicinity of the breached dam where extremely high flow velocities uproot trees and transport considerable sediment and boulders (if present), and generally result in large energy losses.

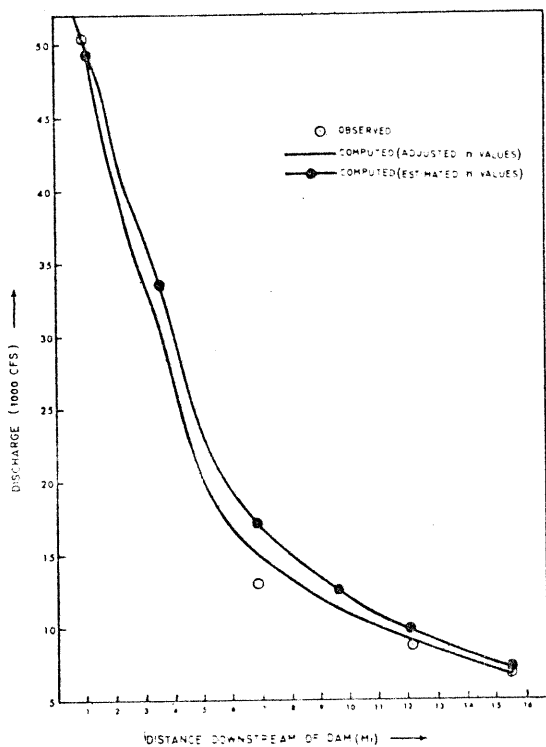


Fig. 10 - PROFILE OF PEAK DISCHARGE FROM BUFFALO CRK. FAILURE

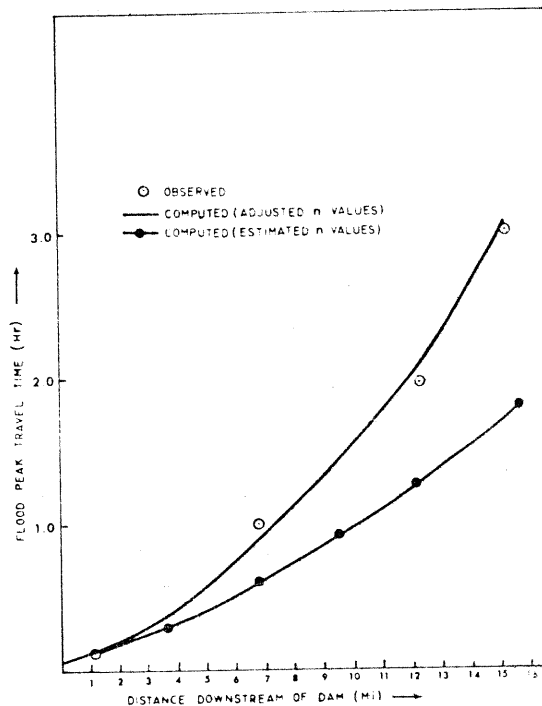


Fig. 11 - TRAVEL TIME OF FLOOD PEAK FROM BUFFALO CREEK FAILURE

A profile of the observed peak flood elevations downstream of the Buffalo Creek coal-waste dam is shown in Fig. 12, along with the computed elevations using adjusted n values. The average absolute error is 1.8 feet and the average arithmetic error is -0.9 foot.

Sensitivities of the computed downstream peak discharges to reasonable variations in the selection of breach parameters (τ , b , and z) are shown in Fig. 13. The resulting differences in the computed discharges diminish in the downstream direction. Like the Teton dam-break flood wave, errors in forecasting the breach are damped-out as the flood advances downstream.

A typical simulation of the Buffalo Creek flood involved 63 Δx reaches, 3.0 hours of prototype time, use of the reservoir storage routing option, and initial time step of 0.002 and 0.005 hour for the supercritical and subcritical downstream reaches, respectively. Computation time for a typical simulation run was 18 seconds (IBM 360/195).

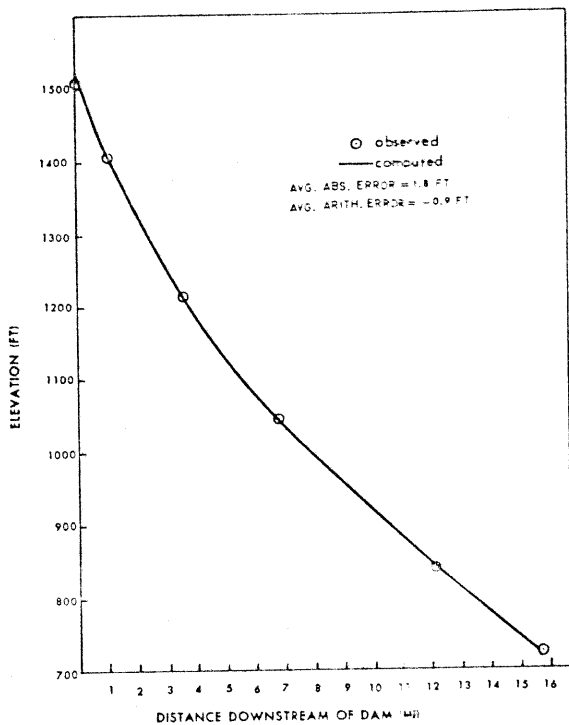


Fig. 12 - PROFILE OF PEAK FLOOD ELEVATION FROM BUFFALO CREEK FAILURE

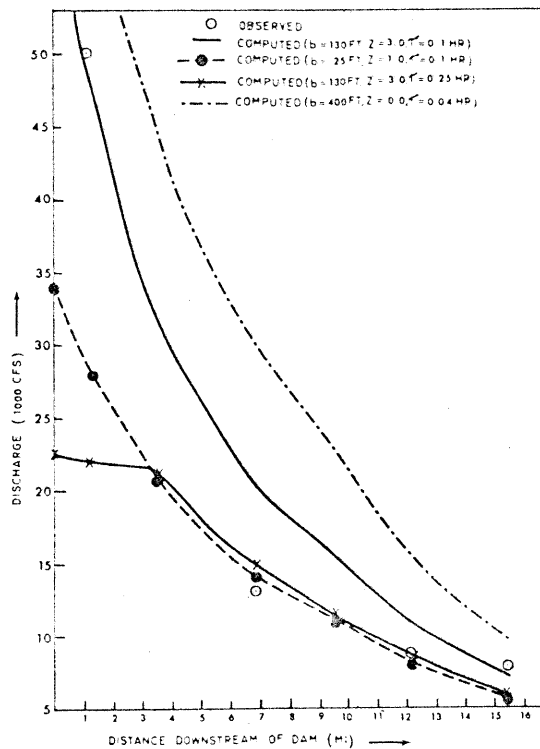


Fig. 13 - PROFILE OF PEAK DISCHARGE FROM BUFFALO CRK. FAILURE SHOWING SENSITIVITY OF VARIOUS INPUT PARAMETERS

5. FLOOD INUNDATION APPLICATIONS

The NWS DAMBRK model is suitable for the following two types of dam-break flood inundation applications: 1) pre-computation of flood peak elevations and travel times prior to a dam failure, and 2) real-time computation of the downstream flooding when a dam failure is imminent or has immediately occurred.

Pre-computations of dam failures enable the preparation of concise graphs or flash flood tables for use by those responsible for community preparedness downstream of critically located dams. The graphs provide information on flood peak elevations and travel times throughout the critical reach of the downstream valley. The variations in the pre-computed values due to uncertainty in the breach parameters (τ and \bar{b}) can be included in the graph. Results obtained using a maximum probable estimate of \bar{b} and a minimum probable estimate of τ would define the upper envelope of probable flood peak elevations and minimum travel times. Similarly, the use of a minimum probable estimated \bar{b} , along with a maximum probable estimate of τ , would define the lower limit of the envelope of probable peak elevations and maximum travel times. In the pre-computation mode, the forecaster can use as much of the capabilities of the DAMBRK model as time and data availability warrant.

Real-time computation is also possible in certain situations where the total response time for a dam-break flood warning exceeds a few hours. An abbreviated data input to DAMBRK with essential input data flagged can be used to quickly compute an approximate crest profile and arrival times. Using available topo maps and a minimum of information on the dam such as its height and storage volume, a real-time forecast can be made within approximately 30 minutes. Pre-computed forecasts could be updated when observations of the extent of the breach are available. This would be valuable in refining the forecast for communities located far downstream where the possibility of flood inundation is questionable and the need for eventual evacuation could be more accurately defined. The data set used to make the real-time update of the pre-computed forecast would be retrieved from a data storage system and the critical parameters therein changed prior to the update simulation run.

The DAMBRK model can also be used to route any specified flow through a river valley. In such applications of the model, the dam breach and reservoir routing data input and computational components are not used.

6. SUMMARY AND CONCLUSIONS

A dam-break flood forecasting model (DAMBRK) is described and applied to some actual dam-break flood waves. The model consists of a breach component which utilizes simple parameters to provide a temporal and geometrical description of the breach. A second component computes the reservoir outflow hydrograph resulting from the breach via a broad-crested weir-flow approximation, which includes effects of submergence from downstream tailwater depths and corrections for approach velocities. Also, the effects of storage depletion and upstream inflows on the computed outflow hydrograph are accounted for through storage routing within the reservoir. The third component consists of a dynamic routing technique for determining the modifications to the dam-break flood wave as it advances through the downstream valley, including its travel time and resulting water surface elevations. The dynamic routing component is based on a weighted, four-point non-linear finite difference solution of the one-dimensional equations of unsteady flow which allows variable time and distance steps to be used in the solution procedure. Provisions are included for routing supercritical flows as well as subcritical flows, and incorporating the effects of downstream obstructions such as road-bridge embankments and/or other dams.

Model data requirements are flexible, allowing minimal data input when it is not available while permitting extensive data to be used when appropriate.

The model was tested on the Teton Dam failure and the Buffalo Creek coal-waste dam collapse. Computed outflow volumes through the breaches coincided with the observed values in magnitude and timing. Observed peak discharges along the downstream valleys were satisfactorily re-

produced by the model even though the flood waves were severely attenuated as they advanced downstream. The computed peak flood elevations were within an average of 1.5 ft and 1.8 ft of the observed maximum elevations for Teton and Buffalo Creek, respectively. Both the Teton and Buffalo Creek simulations indicated an important lack of sensitivity of downstream discharge to errors in the forecast of the breach size and timing. Such errors produced significant differences in the peak discharge in the vicinity of the dams; however, the differences were rapidly reduced as the waves advanced downstream. Computational requirements of the model are quite feasible; CPU time (IBM 360/195) was 0.005 second per hr per mile of prototype dimensions for the Teton Dam simulation, and 0.095 second per hr per mile for the Buffalo Creek simulation. The more rapidly rising Buffalo Creek wave ($\tau = 0.008$ hr as compared to Teton where $\tau = 1.25$ hr) required smaller Δt and Δx computational steps; however, total computation times (Buffalo: 19 sec and Teton: 18 sec) were similar since the Buffalo Creek wave attenuated to insignificant values in a shorter distance downstream and in less time than the Teton flood wave.

ACKNOWLEDGEMENTS

The author would like to gratefully acknowledge the assistance of Frank Dall of HUD in preparing the introduction.

REFERENCES

- Amein, M., and C. S. Fang, 1970: Implicit flood routing in natural channels. Jour. Hydraulic. Div., ASCE, 96, HY12, Dec., pp. 2481-2500.
- Balloffet, A., 1977: Simulation of dam break flooding under normal and probable maximum flood conditions, Proceedings, Dam-Break Flood Modeling Workshop, U.S. Water Resources Council, Washington, D.C., pp. 384-401.
- Balloffet, A., E. Cole, and A. F. Balloffet, 1974: Dam collapse wave in a river, Journ. Hydraul. Div., ASCE, 100, HY5, May, pp. 645-665.
- Baltzer, R., and C. Lai, 1969: Computer simulation of unsteady flows in waterways. Journ. Hydraul. Div., ASCE, 94, HY4, July, pp. 1083-1117.
- Brater, E., 1959: Hydraulics. Civil Engineering Handbook, edited by L. C. Urquhart, Sect. 4, McGraw-Hill Book Co., New York, pp. 4.44-4.60.
- Brevard, J. A., and F. D. Theurer, 1979: Simplified dam-break routing procedure, Technical Release Number 66, U.S. Dept. of Agriculture, Soil Conservation service, Engr. Div., 35 pp.
- Brown, R. J., and D. C. Rogers, 1977: A simulation of the hydraulic events during and following the Teton Dam failure, Proceedings, Dam-Break Flood Modeling Workshop, U.S. Water Resources Council, Washington, D.C., pp. 131-163.
- Chaudhry, Y. M., and D. N. Contractor, 1973: Application of the implicit method to surges in open channels. Water Resour. Res., 9, No. 6, Dec., pp. 1605-1612.

- Chen, C., and L. A. Druffel, 1977: Dam-break flood wave computation by method of characteristics and linearized implicit schemes, Proceedings, Dam-Break Flood Modeling Workshop, U.S. Water Resources Council, Washington, D.C., pp. 312-345.
- Chow, V. T., 1959: Open-channel Hydraulics, McGraw-Hill Co., New York, pp. 476-481.
- Cristofano, E. A., 1965: Method of computing rate for failure of earth fill dams. Bureau of Reclamation, Denver, Colo., April.
- Cunge, J. A., 1975: Rapidly varying flow in power and pumping canals. Unsteady Flow in Open Channels, edited by K. Mahmood and V. Yevjevich, Vol. II, Chapt. 14, Water Resour. Pub., Ft. Collins, Colo., pp. 539-586.
- Davidson, D. D., and B. L. McCartney, 1975: Water waves generated by landslides in reservoirs. Journ. Hydraul. Div., ASCE, 101, HY12, Dec., pp. 1489-1501.
- Davies, W. E., J. F. Bailey, and D. B. Kelly, 1972: West Virginia's Buffalo Creek flood: a study of the hydrology and engineering geology. Geological Survey Circular 667, U.S. Geological Survey, 32 pp.
- De Saint-Venant, Barre, 1871: Theory of unsteady water flow, with application to river floods and to propagation of tides in river channels. Acad. Sci. (Paris) Comptes rendus, 73, pp. 237-240.
- Dressler, R. F., 1954: Comparison of theories and experiments for the hydraulic dam-break wave. Internat. Assoc. Sci. Pubs., 3, No. 38, pp. 319-328.
- Fread, D. L., 1971: Discussion of implicit flood routing in natural channels. M. Amein and C. S. Fang, Journ. Hydraul. Div., ASCE, 97, HY7, July, pp. 1156-1159.
- Fread, D. L., and T. E. Harbaugh, 1973: Transient hydraulic simulation of breached earth dams, Journ. Hydraul. Div., ASCE, 99, HY1, Jan., pp. 139-154.
- Fread, D. L., 1974a: Numerical properties of implicit four-point finite difference equations of unsteady flow. NOAA Tech. Memo. NWS HYDRO-18, U.S. Dept. of Commerce, NOAA, National Weather Service, 38 pp.
- Fread, D. L., 1974b: Implicit dynamic routing of floods and surges in the Lower Mississippi. Presented at AGU Natl. Mtg., Wash., D.C., April, 26 pp.
- Fread, D. L., 1975: Discussion of comparison of four numerical methods for flood routing, R. K. Price, Journ. Hydraul. Div., ASCE, 101, HY3, March, pp. 565-567.
- Fread, D. L., 1976: Flood routing in meandering rivers with flood plains, Proceedings, Rivers '76, Third Ann. Symp. of Waterways, Harbors and Coastal Eng. Div., ASCE, Vol. I, Aug., pp. 16-35.
- Fread, D. L., 1977: The development and testing of a dam-break flood forecasting model, Proceedings, Dam-Break Flood Modeling Workshop, U.S. Water Resources Council, Washington, D.C., 1977, pp. 164-197.
- Fread, D. L., 1978: NWS operational dynamic wave model, Verification of Mathematical and Physical Models in Hydraulic Engineering, Proceedings, 26th Annual Hydraulics Div. Specialty Conf., College Park, Md., Aug., pp. 455-464.
- Gundlach, D. L., and W. A. Thomas, 1977: Guidelines for calculating and routing a dam-break flood, Research Note No. 5, Corps of Engineers, U.S. Army, The Hydrologic Engr. Center, 50 pp.

- Harris, G. W., and D. A. Wagner, 1967: Outflow from breached dams, Univ. of Utah.
- Johnson, F. A., and P. Illes, 1976: A classification of dam failures, Water Power and Dam Construction, Dec., pp. 43-45.
- Keefer, T. N., and R. K. Simons, 1977: Qualitative comparison of three dam-break routing models, Proceedings, Dam-Break Flood Modeling Workshop, U.S. Water Resources Council, Washington, D.C., pp. 292-311.
- Koutitas, C. G., 1977: Finite element approach to waves due to landslides, Journ. Hydraul. Div., ASCE, 103, HY9, Sept., pp. 1021-1029.
- Liggett, J., and J. A. Cunge, 1975: Numerical methods of solution of the unsteady flow equations. Unsteady Flow in Open Channels, edited by K. Mahmood and V. Yevjevich, Vol. I, Chapt. 4, Water Resour. Pub., Ft. Collins, Colo., pp. 89-182.
- Martin, C. S., and J. J. Zovne, 1971: Finite-difference simulation of bore propagation. Journ. Hydraul. Div., ASCE, 97, HY7, July, pp. 993-1010.
- McQuivey, R. S., and T. N. Keefer, 1976: Application of simple dam break routing model. Proceedings, 16th Congress, IAHR, São Paulo, Brazil, July 27-August 1, 1975, Vol. 2, pp. 315-324.
- Middlebrooks, T. A., 1952: Earth-dam practice in the United States, Centennial Transactions, ASCE, Paper No. 2620, pp. 697-722.
- Morris, H. M., and J. M. Wiggert, 1972: Applied Hydraulics in Engineering, The Ronald Press Co., New York, pp. 570-573.
- Preissmann, A., 1961: Propagation of translatory waves in channels and rivers. Paper presented at First Congress of French Assoc. for Computation, Grenoble, Sept. 14-16, Proceedings, AFCAL, pp 433-442.
- Price, J. T., G. W. Lowe, and J. M. Garrison, 1977: Unsteady flow modeling of dam-break waves, Proceedings, Dam-Break Flood Modeling Workshop, U.S. Water Resources Council, Washington, D.C., pp. 90-130.
- Rajar, R., 1978: Mathematical Simulation of dam-break flow, Journ. Hydraul. Div., ASCE, 104, HY7, July, pp. 1011-1-26.
- Ray, H. A., L. C. Kjelstrom, E. G. Crosthwaite, and W. H. Low, 1976: The flood in southeastern Idaho from the Teton Dam failure of June 5, 1976. Unpublished open file report, U.S. Geological Survey, Boise, Idaho.
- Ré, R., 1946: A study of sudden water release from a body of water to canal by the graphical method. Houille Blanche (France), No. 3, pp. 181-187.
- Ritter, A., 1892: The propagation of water waves. Ver. Deutsch Ingenieure Zeitschr. (Berlin), 36, Pt. 2, No. 33, pp. 947-954.
- Sakkas, J. G., and T. Strelkoff, 1973: Dam break flood in a prismatic dry channel, Journ. Hydraul. Div., ASCE, 99, HY12, Dec., pp. 2195-2216.
- Schocklitsch, A., 1917: On waves created by dam breaches. Akad. Wiss. (Vienna) Proc., 126, Pt. 2A, pp. 1489-1514.
- Smith, R. H., 1978: Development of a dynamic flood routing model for small meandering rivers. Ph.D. dissertation, Univ. Missouri-Rolla, 159 pp.
- Stoker, J. J., 1957: Water Waves, Inter-Science Pub., New York, pp. 333-341
- Strelkoff, T., 1970: Numerical solution of Saint-Venant equations. Journ. Hydraul. Div., ASCE, 96, HY1, Jan., pp. 223-252.
- Strelkoff, T., 1970: Numerical solution of Saint-Venant equations. Journ. Hydraul. Div., ASCE, 96, HY1, Jan., pp. 223-252.

- Su, S. T., and A. H. Barnes, 1970: Geometric and frictional effects on sudden releases. Journ. Hydraul. Div., ASCE. 96, HY11, Nov., pp. 2185-2200.
- Terzidis, G., and T. Strelkoff, 1970: Computation of open channel surges and shocks. Journ. Hydraul. Div., ASCE. 96, HY12, Dec., pp. 2581-2610.
- Thomas, W. A., 1977: Calculating and routing of the Teton dam-break flood, Proceedings, Dam-Break Flood Modeling Workshop, U. S. Water Resources Council, Washington, D. C., pp. 198-227.
- U. S. Army Corps of Engineers, 1960: Floods resulting from suddenly breached dams--conditions of minimum resistance, hydraulic model investigation. Misc. Paper 2-374, Report 1, WES, Feb., 176 pp.
- U. S. Army Corps of Engineers, 1961: Floods resulting from suddenly breached dams--conditions of high resistance, hydraulic model investigation. Misc. Paper 2-374, Report 2, WES, Nov., 121 pp.
- U. S. Army Corps of Engineers, 1975: National Program of Inspection of Dams, Vol. I-V, Dept. of the Army, Office of Chief of Engineers, Washington, D. C.
- U. S. Dept. Transportation/Federal Highway Administration, 1978: Hydraulics of Bridge Waterways, Hydraulic Design Series No. 1, Washington, D. C., pp. 45-46.
- Venard, J. K., 1954: Elementary Fluid Mechanics, John Wiley and Sons, New York, pp. 312-325.

- Su, S. T., and A. H. Barnes, 1970: Geometric and frictional effects on sudden releases. Journ. Hydraul. Div., ASCE. 96, HY11, Nov., pp. 2185-2200.
- Terzidis, G., and T. Strelkoff, 1970: Computation of open channel surges and shocks. Journ. Hydraul. Div., ASCE. 96, HY12, Dec., pp. 2581-2610.
- Thomas, W. A., 1977: Calculating and routing of the Teton dam-break flood, Proceedings, Dam-Break Flood Modeling Workshop, U. S. Water Resources Council, Washington, D. C., pp. 198-227.
- U. S. Army Corps of Engineers, 1960: Floods resulting from suddenly breached dams--conditions of minimum resistance, hydraulic model investigation. Misc. Paper 2-374, Report 1, WES, Feb., 176 pp.
- U. S. Army Corps of Engineers, 1961: Floods resulting from suddenly breached dams--conditions of high resistance, hydraulic model investigation. Misc. Paper 2-374, Report 2, WES, Nov., 121 pp.
- U. S. Army Corps of Engineers, 1975: National Program of Inspection of Dams, Vol. I-V, Dept. of the Army, Office of Chief of Engineers, Washington, D. C.
- U. S. Dept. Transportation/Federal Highway Administration, 1978: Hydraulics of Bridge Waterways, Hydraulic Design Series No. 1, Washington, D. C., pp. 45-46.
- Venard, J. K., 1954: Elementary Fluid Mechanics, John Wiley and Sons, New York, pp. 312-325.